

Detection of Fetal Heart Rate Through 3-D Phase Space Analysis From Multivariate Abdominal Recordings

Evangelos C. Karvounis, *Member, IEEE*, Markos G. Tsipouras, *Member, IEEE*,
and Dimitrios I. Fotiadis*, *Senior Member, IEEE*

Abstract—A novel three-stage methodology for the detection of fetal heart rate (fHR) from multivariate abdominal ECG recordings is introduced. In the first stage, the maternal R-peaks and fiducial points (maternal QRS onset and offset) are detected, using band-pass filtering and phase space analysis. The maternal fiducial points are used to eliminate the maternal QRS complexes from the abdominal ECG recordings. In the second stage, two denoising procedures are applied to enhance the fetal QRS complexes. The phase space characteristics are employed to identify fetal heart beats not overlapping with the maternal QRSSs, which are eliminated in the first stage. The extraction of the fHR is accomplished in the third stage, using a histogram-based technique in order to identify the location of the fetal heart beats that overlap with the maternal QRSSs. The methodology is evaluated on simulated multichannel ECG signals, generated by a recently proposed model with various SNRs, and on real signals, recorded from pregnant women in various weeks during gestation. In both cases, the obtained results indicate high performance; in the simulated ECGs, the accuracy ranges from 72.78% to 98.61%, depending on the employed SNR, while in the real recordings, the average accuracy is 95.45%. The proposed methodology is advantageous since it copes with the existence of noise from various sources while it is applicable in multichannel abdominal recordings.

Index Terms—Abdominal ECG, fetal heart rate (fHR), multivariate analysis, phase space analysis.

I. INTRODUCTION

ADEQUATE obstetric care of the pregnant woman and the fetus requires detailed information about their condition during gestation. Doppler ultrasound is the most common tool used in clinical practice for the monitoring of the fetal heart rate (fHR). However, it suffers from major limitations, the most important being that energy is introduced into the uterus from the bulky transducer (containing the ultrasound generation and detection elements) and toward the fetus. Thus, it cannot be

used for long-term monitoring [1]. Fetal scalp electrodes are also used for fetal electrocardiogram (fECG) monitoring, which is an invasive technique. The ECG of a pregnant woman can also be obtained using electrodes placed on the abdomen, and in some cases, on the abdomen and the thorax. The thoracic signals contain primarily the maternal ECG (mECG), with little (if any) contribution from the fECG. On the contrary, the abdominal leads record a composite signal (abdECG), consisting of the contributions from both the mECG and the fECG. Abdominally recorded ECG is a convenient method to derive fHR data, since it is not based on energy emission and is not invasive. The characteristics of fECG can be proven useful in determining if the fetus is developing or being delivered properly. These include an elevated heart rate that indicates fetal stress, cardiac arrhythmia, and ST segment depression, which may indicate acidosis [2].

There are several difficulties in recording the abdECG and, subsequently, extracting the fECG from it. Furthermore, mECG signal carries much more energy than the fECG signal, which is embedded in it [3], [4], depending on the gestational age, the position of the fetus [5], and the positioning of the electrodes (there is no standard electrode positioning for optimal fECG acquisition [6]). Moreover, the fECG will occasionally overlap with mECG, making impossible the detection of the fetal R peaks that overlap with maternal R peaks. In addition, there are several sources of interference noise that cannot be removed by simple frequency band filtering. These include intrinsic noise from the recorder, noise from electrode–skin contact and movement, baseline drift (dc shift), ac interference noise (50 Hz), etc. Uterine contractions distort further the fECG recordings, corrupting them with other electrophysiological signals such as uterine muscle noise, which can be recorded by the uterine electromyogram (EMG) or electrohysterogram (EHG). Finally, possible fetal movements and changes in the conductivity of the maternal volume conductor due to the development of the vernix caseosa layer around the fetus may be introduced in the recordings. These types of noise are typically nonstationary and colored [7]. The range of the spectral components of the mECG and fECG waveforms is 0.3–100 Hz, for the abdominal muscle it is 10–400 Hz, while the frequency components of uterine contractions lie in the range 0.01–0.5 Hz. All these make the problem of fECG and/or fHR extraction from the abdECG a very complex task.

Two major approaches exist in the analysis of fetal electrical activity from abdECG signals: 1) extraction of the fECG from

Manuscript received February 19, 2008; revised June 16, 2008, August 18, 2008, and December 11, 2008. First published February 18, 2009; current version published May 22, 2009. Asterisk indicates corresponding author.

E. C. Karvounis is with the Department of Materials Science and Engineering, University of Ioannina, GR 45110 Ioannina, Greece (e-mail: ekarvuni@cc.uoi.gr).

M. G. Tsipouras is with the Unit of Medical Technology and Intelligent Information Systems, Department of Computer Science, University of Ioannina, GR 45110 Ioannina, Greece (e-mail: markos@cs.uoi.gr).

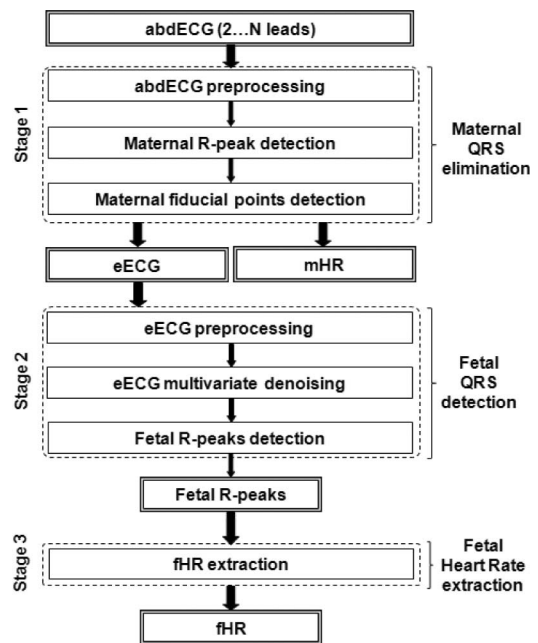
*D. I. Fotiadis is with the Unit of Medical Technology and Intelligent Information Systems, Department of Materials Science and Engineering, University of Ioannina, GR 45110 Ioannina, Greece. He is also with the Biomedical Research Institute—FORTH, GR 45110 Ioannina, Greece (e-mail: fotiadis@cs.uoi.gr).

Color versions of one or more of the figures in this paper are available online at <http://ieeexplore.ieee.org>.

Digital Object Identifier 10.1109/TBME.2009.2014691

the abdECG and, subsequently, identification of the fHR from it, or 2) direct extraction of the fHR. The analysis of the abdECG depends on the scope of the study. The problem of fECG extraction from the abdECG can be formulated as a blind source separation (BSS) problem, since it involves the separation and estimation of the original source waveforms from a sensor array, without knowing the transmission channel characteristics and the sources [8]. The BSS methods are divided into two major groups, the ones that use second-order statistics, using singular value decomposition (SVD) [8]–[10] or principal component analysis (PCA) [8], [11], and those that take advantage of the higher order statistical information contained in the available data, based on independent component analysis (ICA) [8] or BSS in the wavelet domain method [12]. The main disadvantage of the BSS-based methods is that they require a large number of recorded ECG leads [8], [10], [12] in order to obtain satisfactory results (this does not apply to template subtraction); the number of external sensors (leads) must be greater or equal to the number of original sources, and they (the sensors) must record different mixtures of these sources [6]. In addition, such methods fail in precise extraction of the fECG, since in the extracted fECG the contamination from the mECG is easily recognizable [13]. Finally, BSS-based methods suffer from scaling and permutation [8], [14]. Besides BSS-based methods, various signal processing techniques have been developed for the extraction of the fECG signal from composite multichannel recordings, including a combination of PCA and match filtering [15], temporal structure [16], fuzzy logic [9], signal's kurtosis analysis [17], adaptive filtering [3], [11], fractals [18], polynomial networks [19] and neural networks [4]. A recent approach is based on an adaptive neurofuzzy inference system (ANFIS) [20]. In this case, thoracic leads are necessary, which, however, makes the recording phase more complicated. The wavelet transform (WT) has also been proposed, employing biorthogonal quadratic spline wavelet and modulus maxima theory [21], for fECGs processing and noise removal as well as detection of fetal waveforms. In the case of extracting directly the fHR from the abdECG, the proposed methods include matched filtering [1], combination of BSS and heart instantaneous frequency [22], digital filtering combined with adaptive thresholding [23], fuzzy logic [24] and combination of time–frequency (t – f) analysis and wavelet transform [14].

In this paper, we propose a methodology for the automated detection of the fHR and mHR signals, based on the analysis of multichannel abdECG leads. In the first stage, one abdECG is analyzed using a simple filtering procedure. The application leads to a denoised recording that contains primarily the mQRS complexes. The position of the maternal R-peaks is detected using a parabolic fitting approach [25]. The maternal fiducial points (QRS onset and offset) are identified using 3-D phase space analysis [26]–[28]. The maternal fiducial points are used to eliminate the mQRS complexes from the abdECGs, resulting in the eliminated ECG (eECG). In the second stage, multivariate analysis [29]–[31] is applied to reduce the effect of the background (additive) noise in the eECG recordings. Then, 3-D phase space analysis is employed to detect the fQRS complexes and, subsequently, the fetal R-peaks. The fetal R-peaks that overlap



A. Stage 1: Maternal QRS Elimination

In the first stage, the abdECG leads (matrix columns) are analyzed to extract the mHR and the eECG. For this purpose, initially, preprocessing of the abdECG is applied. Then, the parabolic fitting approach [25] and a 3-D phase space analysis are used. The three steps (bandpass filter, parabolic fitting, and 3-D phase space analysis) of the first stage are applied into a single lead of the abdECG (the first column of the abdECG matrix); since all abdECG leads include strong interference from the mECG, one of these leads is sufficient for analysis.

1) *abdECG Preprocessing*: The frequency components of the mQRSs lie in the 4–20 Hz subband [33]. Thus, a linear-phase FIR bandpass filter with these cutoff frequencies is applied, resulting in a filtered signal f . This eliminates components from the abdECG signal, like maternal P and T waves, fECG interference, and noise artifacts.

2) *Maternal R-Peak Detection*: We apply the parabolic fitting technique to the filtered signal f , to detect the maternal R-peaks that are used for the calculation of mHR. A second-degree polynomial is used to fit the f signal inside a sliding window: $f(i) \approx -a^2(l-k) + b$, where k is the sample index of the signal. The polynomial coefficients a and b are fitted, for each k , by minimizing the objective function: $V(a, b) = \sum_{l=k-[0.02*sf]}^{k+[0.02*sf]} w_l (f(i) - (a^2(l-k) + b))^2$, where sf is the sampling frequency and w_l 's are the weighting parameters of the least squares. For each k , a pair $(a(k), b(k))$ is computed. The R peaks correspond to major maximums of the indicator: $\text{ind}(k) = a(k) * b(k)$, corresponding to the amplitude and the curvature of the signal f for sample k .

3) *Maternal Fiducial Points Detection*: To detect the fiducial points in the mQRS complexes, a phase space thresholding method, which is based on 3-D Poincare maps (3-D phase space plot) is employed. Initially, the first (Δf) and the second ($\Delta^2 f$) derivatives of the signal f are calculated. Then, each point $(f(i), \Delta f(i), \Delta^2 f(i))$ is plotted, creating the 3-D phase space plot. The application of the 3-D phase space thresholding method for the identification of the points that belong to the mQRS complexes, is based on the observation that, when applying the 3-D phase space plot to ECG data, the points in the center (Fig. 2) correspond mainly to P and T waves, low-frequency noise activity, and fECG contamination, while the points in the large surrounding torus mainly correspond to the mQRS complexes and sharp noise contamination [7]. The 3-D ellipsoid is defined, using the universal criterion [26]. All points of the phase space plot lying outside this ellipsoid are considered as points in a mQRS complex. The universal criterion is an estimator of the theoretical expected maximum value of N independent, identically distributed samples of a standard normal distribution, defined as: $\lambda\sigma$, where λ is the universal threshold defined as $\lambda = \sqrt{2 \ln N}$ and σ is the standard deviation. The method was originally proposed by Goring and Nikola [26] and modified by Wahl [27].

The universal thresholding approach for the calculation of the ellipsoid axes is based on the assumption that the samples of the noisy signal are normally distributed. However, this assumption does not hold in the case of the abdECG signal, since the

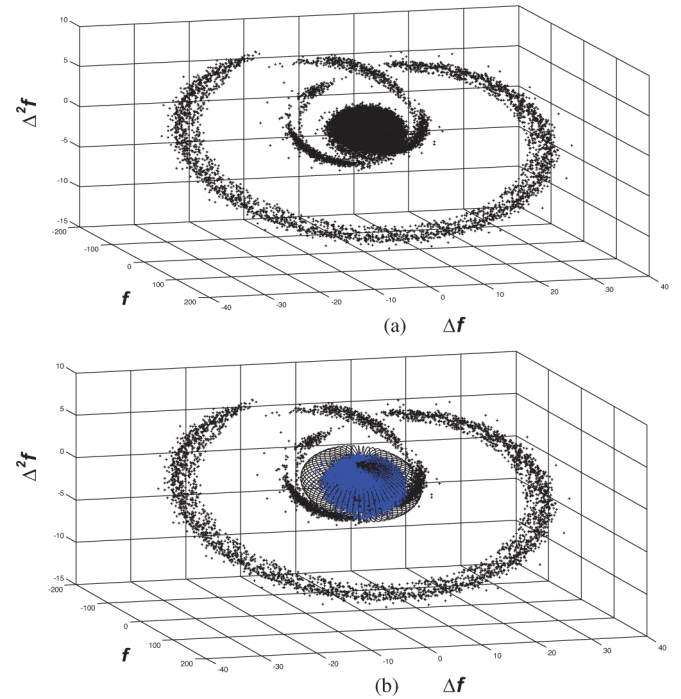


Fig. 2. (a) Three-dimensional phase-space map and (b) ellipsoid used in the maternal QRS-points detection.

signal is contaminated by noise and the assumption of Gaussian distribution is not valid. Thus, we have introduced three parameters (a_1, b_1, c_1) that multiply the universal criterion estimations. Based on this, the procedure for mQRS detection by the phase space analysis is summarized as follows:

- 1) set f to be of zero mean: $f = f - (1/N) \sum_{i=1}^N f(i)$;
- 2) calculate the derivatives Δf and $\Delta^2 f$: $\Delta f(i) = (f(i+1) - f(i-1))/2$ and $\Delta^2 f(i) = (f(i+2) + f(i-2) - 2f(i))/4$ where i is the time sample;
- 3) calculate the angle θ : $\theta = \tan^{-1}((f \cdot \Delta^2 f^T)/(f \cdot f^T))$;
- 4) rotate data:

$$\begin{aligned} & \begin{bmatrix} f^T & \Delta f^T & \Delta^2 f^T \end{bmatrix} \\ &= \begin{bmatrix} f^T & \Delta f^T & \Delta^2 f^T \end{bmatrix} \begin{bmatrix} \cos \theta & 0 & -\sin \theta \\ 0 & 1 & 0 \\ \sin \theta & 0 & \cos \theta \end{bmatrix}; \end{aligned}$$

- 5) calculate λ : $\lambda = \sqrt{2 \ln N}$;
- 6) calculate the standard deviation $\sigma_f, \sigma_{\Delta f}$, and $\sigma_{\Delta^2 f}$ of all three variables $f, \Delta f$, and $\Delta^2 f$;
- 7) calculate the expected maxima $\lambda\sigma_f, \lambda\sigma_{\Delta f}$, and $\lambda\sigma_{\Delta^2 f}$;
- 8) considering an ellipsoid with principal axes $a_1\lambda\sigma_f, b_1\lambda\sigma_{\Delta f}$ and $c_1\lambda\sigma_{\Delta^2 f}$, a point $(f(i), \Delta f(i), \Delta^2 f(i))$ is an outlier (i.e. lies outside this ellipsoid) if: $(f(i)^2/(a_1\lambda\sigma_f)^2) + (\Delta f(i)^2/(b_1\lambda\sigma_{\Delta f})^2) + (\Delta^2 f(i)^2/(c_1\lambda\sigma_{\Delta^2 f})^2) > 1$; each outlier is replaced using spline interpolation.
- 9) the aforesaid steps are applied iteratively until no outliers are identified in step 8.

The aforesaid approach is a generalization of the method proposed in [28], since by setting a_1, b_1 , and c_1 equal to 1, we

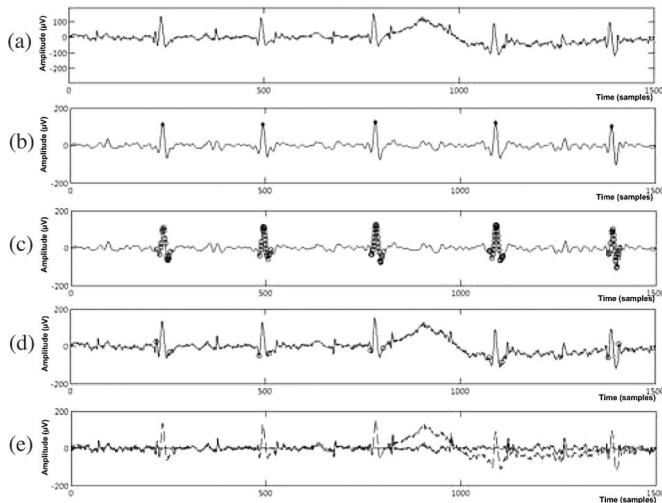


Fig. 3. Working example of the stage 1 of the proposed methodology: (a) abdECG signal, (b) bandpass filtered signal, (c) detected mQRS points, (d) detected maternal fiducial points, and (e) abdECG and eECG signals, with discontinuous and solid lines, respectively.

obtain the axes of the ellipsoid $(\lambda\sigma_f, \lambda\sigma_{\Delta f}, \lambda\sigma_{\Delta^2 f})$, which is the original approach. In our case, we have defined the values of the parameters heuristically to be $a_1 = b_1 = 1$ and $c_1 = 0.8$. A 3-D phase space map and the corresponding ellipsoid are shown in Fig. 2 (i.e., $\Delta^2 f$ versus f and Δf).

The outcomes of both the maternal R-peaks detection technique and the mQRS-points detection technique (points belonging to the mQRSs) are used for the final identification of the maternal fiducial points. For each maternal R-peak, the last consecutive mQRS-point to the left and right define the maternal Q wave start (mQRS onset) and S wave end (mQRS offset), respectively. After the maternal fiducial point detection, the mQRSs are eliminated from the initial abdECG signal (not the filtered one) and spline interpolation between the fiducial points, using a high-order polynomial curve fitting (sixth order) and subtraction from the initial signal, is performed. The interpolation is used in order to avoid pseudospikes at the margins of the mQRSs. The elimination procedure is applied in all abdECG leads, thus resulting to the eECG, which is the final outcome of this stage and it is also represented as an $N \times M$ matrix. A working example of the first stage is presented in Fig. 3, where the initial abdECG signal, the bandpass filtered signal, the detected mQRS points, and the maternal fiducial points as well as the abdECG and eECG are shown.

B. Stage 2: Fetal QRS Detection

In this stage, initially, each lead (column) of the eECG is denoised using two methods: a bandpass filtering and a multivariate denoising procedure, based on multiscale PCA (MSPCA). Next, the fetal R-peaks are detected using the phase space thresholding method. The outcome of this stage is the location of the fetal R-peaks not overlapping with the mQRSs, which are eliminated in stage 1.

1) *eECG Preprocessing*: The frequency components of the fQRSs lie in the 4–80 Hz subband [1], [2], [7], [32], [34]. Thus,

a linear-phase FIR bandpass filter with these cutoff frequencies is applied. This step eliminates noise artifacts from the eECG signal.

2) *eECG Multivariate Denoising*: Noise is also removed using MSPCA. MSPCA combines the ability of PCA to decorrelate the variables by extracting a linear relationship, with that of wavelets to extract deterministic features and decorrelate autocorrelated measurements. MSPCA computes the PCA of the wavelet coefficients at each scale and then combines the results at relevant scales. Due to its multiscale nature, MSPCA performs well in the case of modeling nonstationary data, such as abdECG multivariate recordings [29].

Multivariate denoising [31] is based on MSPCA to suppress several principal components, thus obtaining a denoising effect. The procedure for multivariate denoising is summarized in the following steps.

- 1) Perform the wavelet transform at level L of each lead (column) of eECG: $\{d_k^j, a_L^j\} = \text{WT}(x_j), j = 1, \dots, M, K = 1, \dots, L$, where x_j is the j th lead (column) of eECG after the application of the bandpass filtering, d_k^j are the detail coefficients of lead j at level k , and a_L^j are the approximation coefficients of lead j .
- 2) Apply robust PCA (RPCA) [30] in the D_1 matrix: compute $\hat{\Sigma}_\varepsilon$, the estimator of the noise covariance matrix defined as $\hat{\Sigma}_\varepsilon = \text{mcd}(D_1)$, where mcd is the minimum covariance determinant estimator [31] and D_1 is the matrix of details of all leads at level 1 ($D_1 = [d_1^j], j = 1, \dots, M$). Compute V such that $\hat{\Sigma}_\varepsilon = V\Lambda V^T$, where $\Lambda = \text{diag}(\lambda_j), j = 1, \dots, M$. Apply thresholding to each matrix of details after change of basis: $D_k V, k = 1, \dots, L$, where $D_k = [d_k^j], j = 1, \dots, M$. Thresholding is applied using $\sqrt{2\lambda_j \ln(N)}, j = 1, \dots, M$ (N is the number of samples) as threshold for each of the M columns of $D_k V$. We obtain finally the simplified matrices of details $\hat{D}_k, k = 1, \dots, L$.
- 3) Perform PCA on the matrix of approximations A_L ($A_L = [a_L^j], j = 1, \dots, M$, thus A_L is an $N \times M$ matrix) and select the appropriate number of useful principal components, using Kaiser's rule [31], resulting in \hat{A}_L . Kaiser's rule retains components associated with eigenvalues exceeding the mean of all eigenvalues.
- 4) Reconstruct the denoised eECG matrix, from all the detail matrices ($\hat{D}_k, k = 1, \dots, L$) and the approximation matrix (\hat{A}_L), by changing the basis using V^T and inverting the wavelet transform.
- 5) Perform PCA on the denoised eECG and select the appropriate number of useful principal components, using the Kaiser's rule.

The proposed procedure generalizes univariate denoising and captures the attractive property of dimensionality reduction of the MSPCA scheme leading to an additional denoising effect [31]. The multivariate denoising procedure only is shown in Fig. 4.

In our application, the parameters of the multivariate denoising were selected as follows: in the first step, wavelet Daubechies 4 function was chosen while six levels of decomposition were

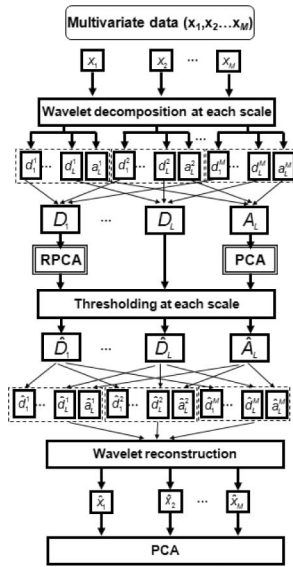


Fig. 4. Flowchart of the multivariate denoising technique.

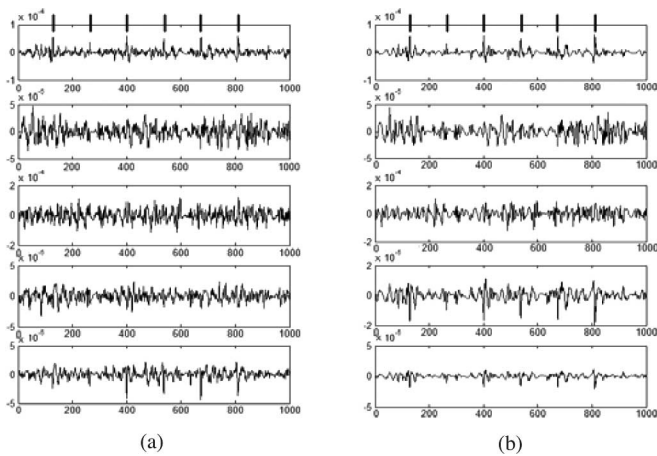


Fig. 5. (a) Five leads of the simulated signal (SNR = -5 dB) and (b) the corresponding signals after the application of the multivariate denoising analysis.

used ($L = 6$). The minimum covariance determinant estimator was calculated based on D_1 , since it mainly contains the noise coefficients, using a subset including 75% of the available data. Selection of principal components in steps 3 (approximations in the wavelet domain) and 5 (PCA after wavelet reconstruction) is made selecting the components using Kaiser’s rule. Fig. 5 presents an example of the multivariate denoising application on the five leads of an eECG signal. The vertical bold lines at the top of the figure indicate the true positions of the fetal R-peaks. The multivariate denoising eliminates noise components without affecting the areas of interest (fetal R-peaks) [31].

3) *Fetal R-Peak Detection*: The denoised eECG is used to detect the fetal R-peaks that do not overlap with mQRSs. The phase space thresholding is applied in each lead of the denoised eECG, thus detecting all spikes that are possible fetal R-peaks. This procedure results in M sets of points (one for each lead)

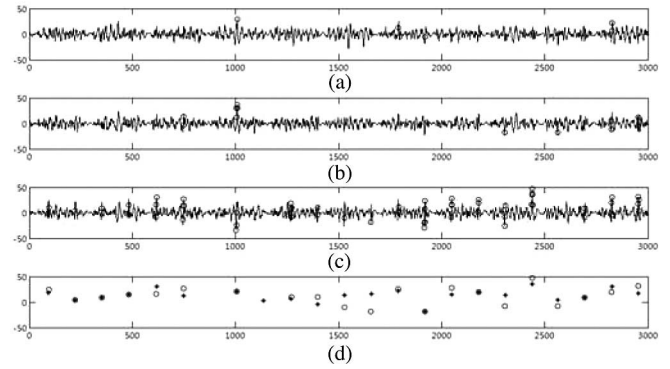


Fig. 6. (a)–(c) Fetal QRS points (denoted with circles on the signal) detected in three leads of the signal and (d) all detected points for the three leads merged in one single lead (denoted with circles “o”) and the annotated fetal R-peaks (with asterisk “*”), not including fetal R-peaks that overlap with mQRSs.

that are merged into a single set of points. Merging is performed in a straightforward manner; the final set of points is the union of the sets resulting for each lead. Based on this new set of points, the detection of the fetal R-peaks is carried out as follows: if, in a window of 20 consecutive samples, more than two samples are detected from the phase space analysis, then the one corresponding to the absolute maximum value is considered as fetal R-peak. The length of the window is chosen to be 20 points (i.e., approximately 66 ms at 300 Hz sampling rate), due to the fact that the fQRS maximum length changes with respect to the week of gestation; the records included in this study were acquired up to the 34th week of gestation, for which the maximum fQRS length is approximately 65 ms [5], [13]. An example of the merging and the fetal R-peak detection procedures is presented in Fig. 6. The multiple circles represent the fetal QRS points detected after application of phase space thresholding in each lead. The plus “*” signs in trace (d) correspond to the annotated fetal R-peaks position (not-including overlapped fetal R-peaks) and they are not presented in plots (a)–(c).

These are plotted only for comparison reasons between detected (denoted with “o”) and annotated fetal R-peaks (denoted with “*”). Parameters are again introduced in the phase space analysis (a_2 , b_2 , and c_2). Those are automatically computed using an estimation of the SNR of the examined abdECG signal, as described in Section V.

C. Stage 3: fHR Extraction

In the first stage of the methodology, the mQRSs are eliminated from the abdECG recordings. However, during this procedure, all fetal R-peaks that overlap with the mQRSs are eliminated as well. Thus, a third stage is employed in order to estimate these fetal R-peaks. The results from stage 2 (fetal R-peaks that do not overlap with mQRSs) and stage 3 (fetal R-peaks that overlap with mQRSs) are combined to provide the fHR.

1) *fHR Extraction*: The fetal R-peaks detected in stage 2 are used to compute the fetal RR-interval signal (fRR). Then, the histogram of the fRR signal is calculated. In Fig. 7(a), a single lead of the abdECG recording is presented, while the

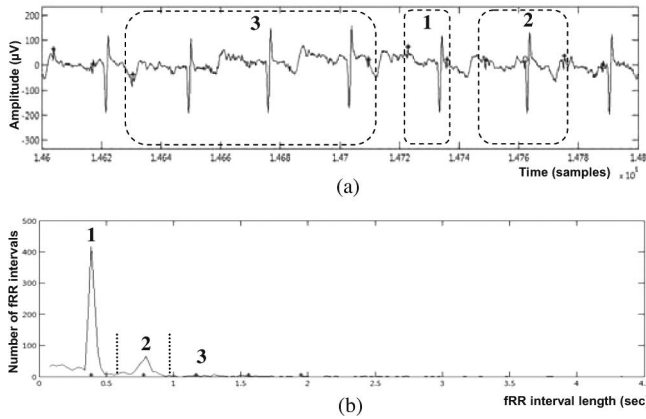


Fig. 7. Fetal heart rate extraction: (a) The abdECG signal: with “*” we denote the fQRSs and with “o” we denote the overlapped fQRSs. (b) Histogram of the signal in Fig. 2(a). In the histogram, area 1 denotes the “basic” fRR interval length (t_{RR}), area 2 denotes “double” fRR interval length ($2t_{RR}$), and area 3 denotes “multi” fRR interval length.

histogram of the fRR signal is presented in Fig. 7(b). The time corresponding to the first peak of the histogram is considered as the “basic” fRR interval length (t_{RR}), and based on this, the $2t_{RR}$ is calculated; both t_{RR} and $2t_{RR}$ are shown in the histogram [Fig. 7(b)] with asterisks (*). Using t_{RR} and $2t_{RR}$, the following procedure is applied.

- 1) All fRR intervals with length $t \in [0, t_{RR} + t_{RR}/2]$ are considered as “normal” fRR intervals and no further processing is applied on them. This time interval is denoted as “1” in Fig. 7(b) while a “normal” fRR interval is denoted with “1” in Fig. 7(a).
- 2) All fRR intervals with length $t \in [2t_{RR} - t_{RR}/2, 2t_{RR} + t_{RR}/2]$ are considered as “double” fRR intervals, i.e., fRR intervals that include one lost fetal R-peak. This time interval is denoted as “2” in Fig. 7(b). The “double” fRR intervals are split in two fRR intervals, considering a fetal R-peak in the center of the “double” fRR interval. This procedure is conducted only if this center is inside an mQRS complex (detected and eliminated in stage 1). A “double” fRR interval is denoted with “2” in Fig. 7(a).
- 3) All fRR intervals with length $t > 2t_{RR} + t_{RR}/2$ are considered as “multi” fRR intervals, i.e., fRR intervals that include two or more lost fetal R-peaks. This time interval is denoted as “3” in Fig. 7(b). The “multi” fRR intervals are considered as highly “noisy” areas of the abdECG signal and no correction process is performed. A “multi” fRR interval is denoted with “3” in Fig. 7(a).

The results extracted in the second stage (positions of fetal R-peaks that do not overlap with maternal QRSs) and the third stage (positions of fetal R-peaks that do overlap with maternal QRSs) are merged in order to extract the fHR.

III. COMPARATIVE STUDY

We compare the proposed methodology with five other approaches already presented in the literature.

- 1) A t-f-based methodology [14] that employs the abdECG signal is used. The methodology follows a three-stage

schema: mQRS detection and elimination, fetal R-peak detection, and detection of the fetal R-peak that overlaps with the maternal QRSs. The methodology is evaluated for the initial abdominal recordings, using mQRS cancellation.

- 2) A parabolic fitting [25] algorithm that takes into account the amplitude and the curvature of the ECG signal. A 20 ms sliding window is used as fQRS is almost half of the length of mQRS [5]. We have also used an algorithm for the correction of erroneous R–R intervals [35].
- 3) A method based on template matching [35] using the parameters proposed. It includes formation of the initial template, subtraction of average from the template, template updating, and rejection of noisy QRS complexes.
- 4) A QRS detection technique based on a smoothed version of the nonlinear energy operator (SNEO) has been applied [36]. We used the parameters proposed in [36] including the procedure for correction of the possible presence of false positives or false negatives.
- 5) Finally, an ICA algorithm is tested. For the implementation, we employed the Hyvarinen’s fixed-point algorithm (Fast ICA) algorithm [37], a non-Gaussianity-based ICA algorithm appropriate for fECG detection. The fetal QRS complexes are accurately detected by finding the maxima, using a threshold on 70%, of the cross correlation of the signal with QRS templates [14]. Correction analysis [36] is applied in the final step.

The t-f analysis is applied in the initial abdECG recordings while parabolic fitting, template matching, SNEO, and Fast-ICA approaches in the eECG signals without our third stage. The Fast-ICA is applied in the eECG signals and the correlation procedure in the extracted independent components.

IV. DATASET

The evaluation of the proposed methodology is based on both simulated and real abdECG recordings. The simulated signals are generated using a 3-D dynamic model of the electrical activity of the heart [7], while the real signals are obtained from the University of Nottingham database [1].

A. Simulated Abdominal ECG Data

Simulated abdECG signals are generated using the dynamical model developed by Sameni *et al.* [7], [32]. The signals are generated from a single-dipole heart model that is then related to the body surface potentials through a linear model that accounts for the temporal movements and rotations of the cardiac dipole, together with a realistic ECG noise model. Three types of noise are included in the signals: baseline wander (BW), muscle artifact (MA), and electrode movement (EM). The proposed model is generalized especially to maternal and fetal ECG mixtures, recorded from the thorax and abdomen of pregnant women. Our approach is based on the analysis of abdominal recordings only; thus, thorax recordings are excluded. For the evaluation of our methodology, we have created simulated multichannel abdominal signals for five channels that correspond to recordings of five abdominal leads. The recordings have duration 5 min

each, while the sampling frequency was 300 Hz. We tested our methodology using various SNRs: -5 , -2 , 0 , 2 , 5 , and 10 dB. Thus, the simulated recordings dataset includes six five-channel recordings.

B. Real ECG Data

We use signals that are obtained from a database created at the University of Nottingham [1]. They have used a recorder developed by them. The ECG signals in this dataset were recorded from three different skin electrodes located at different points of a pregnant woman's abdomen with a sampling frequency of 300 Hz. A reference signal is also acquired from an electrode placed on the mother's abdomen by a low-noise, general-purpose electrophysiological recorder. The recordings are digitized using a 12-bit A/D converter. The measurements are simultaneously recorded from all three channels. The abdECG recordings are obtained between the 20th and 34th week of gestation. The recorder configured with a gain of 7800 and bandwidth of 4–100 Hz (fECG frequency range). Thus, uterine activity components and high-frequency abdominal muscle artifacts are removed, along with low-frequency activity of the mECG and fECG. However, this does not affect the proposed method since we focus on the mHR and fHR extraction. The dataset includes 13 recordings of three channels with duration 15 min. The names of the recordings are represented as $w_{\text{(Patient_Code)}}_{\text{(Gestation_Week)}}$. The annotation of the fetal R-peaks in the recorded signals was performed by an expert cardiologist.

V. RESULTS

Initially, each of the denoising procedures of the second stage (eECG preprocessing and eECG multivariate denoising) was evaluated. This was performed using an SNR estimator: $eSNR = 10 \log((s^T s) / ((x - s)^T (x - s)))$, where $eSNR$ is the estimated SNR, x is the signal, and s is the signal of interest (thus $x - s$ is the noise). The aforesaid is applied to the simulated signals in three instances.

- 1) To the initial signal, which is the eECG generated from stage 1. In this case, $x = x_{\text{initial}} = \text{eECG}$ and s that are known.
- 2) To the filtered signal, which is the eECG after the application of the bandpass filter. In this case $x = x_{\text{initial}}$ and $s = x_{\text{filtered}}$.
- 3) To the final signal, which is the eECG after both denoising procedures (bandpass filter and multivariate denoising). In this case, $x = x_{\text{filtered}}$ and $s = x_{\text{filtered_denoised}}$.

The results of the eSNR of the initial, filtered, and final signals are presented in Table I (average of all five leads), and they indicate that both denoising procedures improve the eSNR of the eECG generated from the simulated signals. A visual example of the eECG preprocessing and eECG multivariate denoising in a real recording ($w_{\text{MJ}_{24}}$) is shown in Fig. 8.

The application of the proposed methodology to a single abdECG recording, either simulated or real, results in a set of detected fetal R-peaks. Three measures are used for the evaluation: sensitivity $Se = TP / (TP + FN)$, positive di-

TABLE I
ESTIMATED SNR (eSNR) FOR DENOISING PROCEDURES OF
SECOND STAGE

Signals	Estimated eSNR		
	Initial (eECG)	Filtered (after band-pass filtering)	Final (after band-pass filtering & multivariate denoising)
1 (-5)	-31.08	-17.88	7.854
2 (-2)	-28.08	-17.49	9.81
3 (0)	-26.08	-16.61	12.72
4 (2)	-24.08	-16.14	7.53
5 (5)	-21.08	-15.60	3.46
6 (10)	-16.28	-12.34	4.92

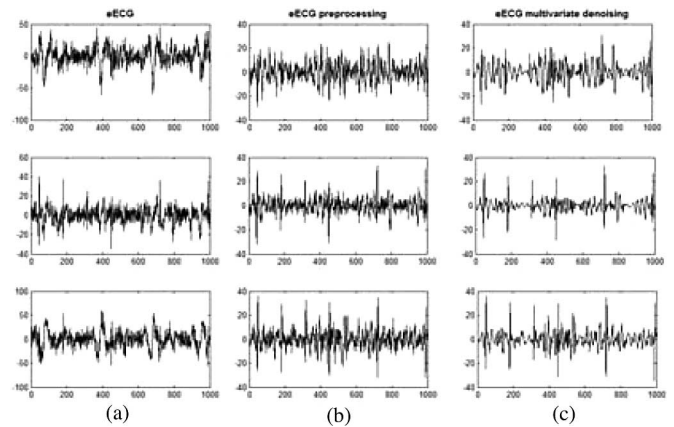


Fig. 8. Working example of the stage 1 of the proposed methodology in a real recording: (a) eECG signal, (b) bandpass filtered signal, (c) bandpass and filtered signal after multivariate denoising.

agnostic value $PDV = TP / (TP + FP)$, and accuracy $Acc = TP / (TP + FP + FN)$, where TP is the number of the true-detected fetal R-peaks, FP is the number of false-detected fetal R-peaks, and FN is the number of not-detected fetal R-peaks. A detected fetal R-peak is considered as true positive if it lies at a distance that is less than 11 points from a fetal R-peak.

Initially, the proposed methodology was evaluated using the six simulated signals and the obtained results are presented in Table II. For each recording, the duration along with TP , FP , FN , Se , PDV , and Acc results are presented. The values of the parameters a_2 , b_2 , and c_2 are set to 1 ($a_2 = b_2 = c_2 = 1$), thus obtaining the original axes of the ellipsoid (universal threshold approach). The average Se , PDV , and Acc are 97.29%, 71.28%, and 69.88%, respectively. Then, we perform parameter analysis, varying a_2 , b_2 , and c_2 in the range of: $a_2, b_2 \in \{0.5, 0.6, \dots, 1.5\}$ and $c_2 \in \{1, 1.5, 2, 2.5\}$. Based on these, the best results are obtained for $(a_2, b_2, c_2) = (1, 1.4, 1.5)$. The corresponding results obtained using these parameter values are presented in Table III. In this case, the average Se , PDV , and Acc are 96.36%, 94.94%, and 92.02%, respectively. Table IV presents the best result, in terms of TP , FP , FN , Se , PDV , and Acc obtained for each of the simulated signals. Also, the values of the parameters a_2 , b_2 , and c_2 , for which the methodology obtained the best accuracy (best Acc), are included in the table. These values range in the intervals $[1.1, 1.5]$, $[1.0, 1.5]$, and $[2.0, 2.5]$ for a_2 , b_2 , and c_2 , respectively. It should be mentioned

TABLE II
OBTAINED RESULTS FROM APPLICATION OF PROPOSED METHODOLOGY TO SIMULATED SIGNALS USING $(a_2, b_2, c_2) = (1, 1, 1)$ (UNIVERSAL THRESHOLD APPROACH)

Signals		Results				
Recording (SNR dB)	TP	FP	FN	Se(%)	PDV(%)	Acc(%)
1 (-5)	637	367	14	97.85	63.45	62.57
2 (-2)	633	284	18	97.24	69.03	67.70
3 (0)	614	229	37	94.32	72.84	69.77
4 (2)	637	248	14	97.85	71.98	70.86
5 (5)	637	211	14	97.85	75.12	73.90
6 (10)	642	211	9	98.62	75.26	74.48
Total	3800	1550	106	97.29	71.28	69.88

TABLE III
OBTAINED RESULTS FROM APPLICATION OF PROPOSED METHODOLOGY TO SIMULATED SIGNALS USING $(a_2, b_2, c_2) = (1.0, 1.4, 1.5)$ (PARAMETER ANALYSIS)

Signals		Results				
Recording (SNR dB)	TP	FP	FN	Se(%)	PDV(%)	Acc(%)
1 (-5)	527	73	124	80.99	87.79	72.78
2 (-2)	646	50	5	99.3	92.76	92.16
3 (0)	642	41	9	98.59	93.96	92.72
4 (2)	646	14	5	99.3	97.92	97.24
5 (5)	651	9	0	100	98.61	98.61
6 (10)	651	9	0	100	98.61	98.61
Total	3763	196	143	96.36	94.94	92.02

TABLE IV
OBTAINED RESULTS FROM APPLICATION OF PROPOSED METHODOLOGY TO SIMULATED SIGNALS (BEST ACC)

Signals		Results					Parameters
Recording (SNR dB)	TP	FP	FN	Se(%)	PDV(%)	Acc(%)	$a_2 - b_2 - c_2$
1 (-5)	561	105	90	86.18	84.23	74.21	1.1-1.0-2.0
2 (-2)	643	11	8	98.77	98.32	97.13	1.1-1.0-2.0
3 (0)	648	5	3	99.54	99.23	98.78	1.2-1.3-2.5
4 (2)	648	4	3	99.54	99.39	98.93	1.3-1.3-2.5
5 (5)	650	1	1	99.85	99.85	99.69	1.4-1.4-2.5
6 (10)	651	0	0	100	100	100	1.5-1.5-2.5
Total	3801	126	105	97.31	96.84	94.79	

that the results presented in Table IV and the corresponding values of $a_2, b_2,$ and c_2 are obtained using the fQRS annotation of the simulated signals; thus, there is no automated technique to estimate the values of the $a_2, b_2,$ and c_2 parameters and, subsequently, obtain the results presented in Table IV. However, the association between the SNR of the simulated signals and the values of the $a_2, b_2,$ and c_2 parameters, shown in Table III, will be utilized in order to develop a technique for the estimation of $a_2, b_2,$ and c_2 , based on an SNR estimation of the real recordings.

The real recordings were subsequently used for evaluation. Table V presents the results obtained for $(a_2, b_2, c_2) = (1, 1, 1)$ (universal threshold criterion). The average Se, PDV, and Acc are 96.01%, 85.18%, and 82.3%, respectively. Again, parameter analysis is performed for the $a_2, b_2,$ and c_2 parameters and the best results are obtained for $(a_2, b_2, c_2) = (1.1, 1.3, 1)$. The corresponding results obtained using these values are presented in Table VI. We present results for each recording, since the amplitude of fECG signals changes during pregnancy period

TABLE V
OBTAINED RESULTS FROM APPLICATION OF PROPOSED METHODOLOGY TO REAL RECORDINGS USING $(a_2, b_2, c_2) = (1, 1, 1)$ (UNIVERSAL THRESHOLD APPROACH)

Signals		Results				
Recording (SNR dB)	TP	FP	FN	Se(%)	PDV(%)	Acc(%)
w_HK_24	1975	202	31	98.45	90.72	89.45
w_HK_28	1860	394	70	96.37	82.52	80.03
w_HK_34	1595	280	46	97.20	85.07	83.03
w_LD_20	1526	336	61	96.16	81.95	79.36
w_TA_20	1902	747	95	95.24	71.80	69.31
w_WM_20	2833	553	312	90.08	83.67	76.61
w_WM_24	1968	397	80	96.09	83.21	80.49
w_MJ_20	2162	379	63	97.17	85.08	83.03
w_MJ_24	2122	567	78	96.45	78.91	76.69
w_LD_32	1802	216	49	97.35	89.30	87.18
w_AW_20	2043	135	70	96.69	93.80	90.88
w_LG_24	1892	217	148	92.75	89.71	83.83
w_ME_20	1947	178	37	98.14	91.62	90.06
Total	25627	4601	1140	96.01	85.18	82.30

TABLE VI
OBTAINED RESULTS FROM APPLICATION OF PROPOSED METHODOLOGY TO REAL RECORDINGS USING $(a_2, b_2, c_2) = (1.1, 1.3, 1.0)$ (PARAMETER ANALYSIS)

Signals		Results				
Recording (SNR dB)	TP	FP	FN	Se(%)	PDV(%)	Acc(%)
w_HK_24	1982	103	24	98.80	95.06	93.98
w_HK_28	1891	155	39	97.98	92.42	90.70
w_HK_34	1563	67	78	95.25	95.89	91.51
w_LD_20	1556	142	31	98.05	91.64	89.99
w_TA_20	1937	491	60	97.00	79.78	77.85
w_WM_20	3084	259	61	98.06	92.25	90.60
w_WM_24	2008	168	40	98.05	92.28	90.61
w_MJ_20	2119	91	106	95.24	95.88	91.49
w_MJ_24	2184	96	16	99.27	95.79	95.12
w_LD_32	1768	63	83	95.52	96.56	92.37
w_AW_20	1950	55	163	92.29	97.26	89.94
w_LG_24	1515	130	525	74.26	92.10	69.82
w_ME_20	1901	60	83	95.82	96.94	93.00
Total	25458	1880	1309	95.04	93.37	89.00

and depends on the gestation week. It increases during the first 25 weeks of gestation, experiences a marked minimum toward the 32nd week, and increases again afterwards. Based on the results obtained from the parameter analysis performed using the simulated signals, we can compute the values of the $a_2, b_2,$ and c_2 for the real recordings. For each of the $a_2, b_2,$ and c_2 parameters, a curve is extracted from the parameter analysis of simulated signals (Table IV), representing the value of the parameter versus the SNR of the simulated signal. The three curves are presented in Fig. 9. Then, for each real recording, its SNR is estimated as

$$ecSNR = p_1 \times 10 \log((s^T s) / ((x - s)^T (x - s))) + p_2$$

where $ecSNR$ is the estimated and corrected SNR, x is the recording, s is the signal of interest (obtained from filtering the x signal in the range 4–80 Hz), and p_1 and p_2 are the correction parameters. The correction parameters are introduced since the eSNR does not take into account the overlapping of the maternal and fetal spectra in the range 4–80 Hz. The calculation

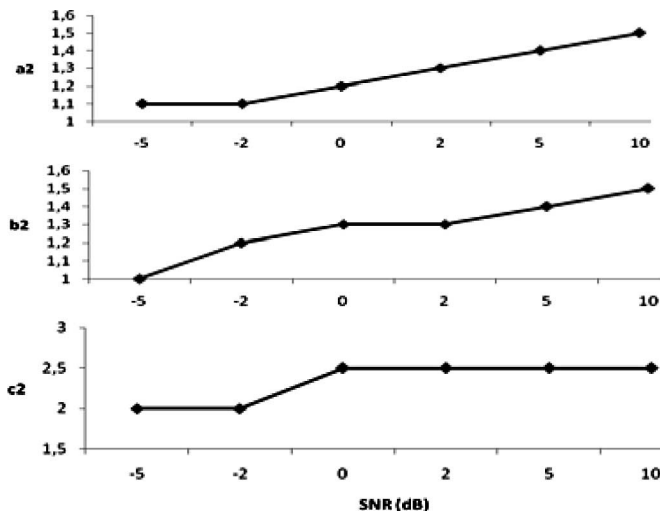


Fig. 9. Parameter (a_2 , b_2 , and c_2) versus SNR curves obtained from parameter analysis using the simulated signals.

of the parameters p_1 and p_2 is based on the fact that a linear dependence is obtained between actual SNR and the eSNR of the simulated abdECGs. The calculation is made using least mean squares. Based on the ecSNR of the real recordings (average of all leads), the values of the parameters are defined using linear interpolation in each curve. For each of the recordings, the estimated SNR, the a_2 , b_2 , and c_2 values estimated using the aforesaid technique, and the results obtained from the proposed methodology using these values, are presented in Table VII. Again, the results are presented in detail for all cases in order to show the variation of the accuracy for different ecSNR values and different weeks of gestation.

A graphic representation of the obtained results in terms of Acc is presented in Figs. 10 and 11, for the simulated signals and the real recordings, respectively. For the simulated signals, the results from the universal threshold approach (Table II), parameter analysis (Table III), and the best Acc (Table IV), are presented. For the real recordings, the results from the universal threshold approach (Table V), parameter analysis (Table VI), and from the parameter estimation (Table VII) are included.

The contribution of each of the processing stages of the proposed methodology is also evaluated. For this reason, results in terms of Acc are obtained for four intermediate stages of our methodology: 1) using only the bandpass filter from the second stage (i.e., without performing multivariate denoising) and without employing the third stage (i.e., estimation of the fetal R-peaks that overlap with the mQRSs); 2) using only the bandpass filter from the second stage (i.e., without performing multivariate denoising) and employing the third stage; 3) using both noise elimination steps (bandpass filtering and multivariate denoising) and without the employment of the third stage, and 4) using both noise elimination steps and employment of the third stage. The results obtained in each case are presented in Fig. 12(a) and (b) for the simulated signals and the real recordings, respectively, while results from the overall methodology are presented in Fig. 12(c). The results indicate that each of the employed processing techniques improves the performance

of the proposed methodology. The effect of the noise removal techniques is more evident in signals with low SNR. Also, the third stage increases significantly the results of QRS detection from the second stage.

VI. DISCUSSION

A methodology for the automated fHR extraction from the abdECG recordings is presented. The method is based on the 3-D phase space analysis of multivariate abdECG recordings and it includes three stages. The proposed methodology has been evaluated using two datasets that contain simulated and real abdECG recordings, respectively.

The results obtained from the parameter analysis using the simulated signals (Table III) indicate that the method is very effective. The accuracy in detecting the fetal R-peaks ranges from 72.78% to 98.61%, with mean value 92.02% and standard deviation 9.84%. The accuracy increases monotonically with respect to the SNR, as shown in Fig. 10. From the obtained results, it is obvious that the proposed methodology is able to address the problem of fetal R detection and fHR extraction very efficiently; when dealing with signals of approximately -2 db SNR or larger, the average accuracy for the simulated signals with $\text{SNR} \geq -2$ db (signals 2–6) is 95.87%. Compared to the results obtained using the universal threshold approach (Table II), the accuracy is increased by 25.99%. The parameter analysis performed using the simulated signals indicate that the larger the SNR of the simulated signal, the larger are the values of the a_2 , b_2 , and c_2 (Table IV). The value of the parameter c_2 does not appear to have a major impact on the accuracy; however, slightly better results are obtained using the larger values of c_2 (2 or 2.5) employed in this analysis.

Linear interpolation on results obtained by the simulated signals is used to estimate a_2 , b_2 , and c_2 for the real signals. Based on this, the values of the parameters can be set in order to more accurately reflect the properties of the examined signal, with respect to its SNR. This is clearly demonstrated from the obtained results: the average accuracy obtained for all real recordings using the parameter estimation technique is 95.45%, while the respective result using parameter analysis is 89% (6.45% difference), and the one using the universal criterion approach is 82.3% (13.15% difference). This performance increase caused by the use of the aforesaid parameter estimation approach is well justified, since: 1) the universal criterion approach is based on the assumption that the examined signal follows normal distribution; 2) the parameter analysis defines a single set of parameters for all real recordings, without taking under consideration the SNR of each signal. Thus, by using the parameter estimation approach, which obtains different parameter values for each signal based on its SNR estimation, the 3-D phase space analysis (fetal R-peak detection step) optimally adjusts to each signal. This is clearly demonstrated in the obtained results (Table VII) and in Fig. 11, where for all real recordings, the accuracy obtained using parameter estimation is equal or better than the one obtained from the parameter analysis. The w_LG_24 presents high level of noise (probably due to electrode movement) located in a 2 min window of the recording; thus, the number of false-detected fetal

TABLE VII
OBTAINED RESULTS FROM APPLICATION OF PROPOSED METHODOLOGY TO REAL RECORDINGS (PARAMETER ESTIMATION)

Signals	Recording (SNR dB)	SNR estimation	Results					Parameters	
			TP	FP	FN	Se(%)	PDV(%)	Acc(%)	$a_2 - b_2 - c_2$
w_HK_24	2.81 db		1950	15	56	97.21	99.24	96.49	1.33 - 1.5 - 2.5
w_HK_28	9.72 db		1920	36	10	99.48	98.16	97.66	1.49 - 1.5 - 2.5
w_HK_34	-4.54 db		1587	46	54	96.71	97.18	94.07	1.1 - 1.05 - 2.0
w_LD_20	-4.74 db		1570	41	17	98.93	97.45	96.44	1.1 - 1.03 - 2.0
w_TA_20	9.46 db		1980	44	17	99.15	97.83	97.01	1.49 - 1.5 - 2.5
w_WM_20	5.6 db		3136	18	9	99.71	99.43	99.15	1.41 - 1.5 - 2.5
w_WM_24	13.45 db		2016	55	32	98.44	97.34	95.86	1.5 - 1.5 - 2.5
w_MJ_20	-4.54 db		2197	32	28	98.74	98.56	97.34	1.1 - 1.5 - 2.5
w_MJ_24	-4.86 db		2177	5	23	98.95	99.77	98.73	1.1 - 1.0 - 2.0
w_LD_32	-4.97 db		1823	34	28	98.49	98.17	96.71	1.1 - 1.0 - 2.0
w_AW_20	-4.92 db		2038	122	75	96.45	94.35	91.19	1.1 - 1.0 - 2.0
w_LG_24	-3.21 db		1970	227	70	96.57	89.67	86.90	1.1 - 1.18 - 2.0
w_ME_20	-4.9 db		1906	59	78	96.07	97.00	93.29	1.1 - 1.0 - 2.0
Total			26270	734	497	98.07	97.24	95.45	

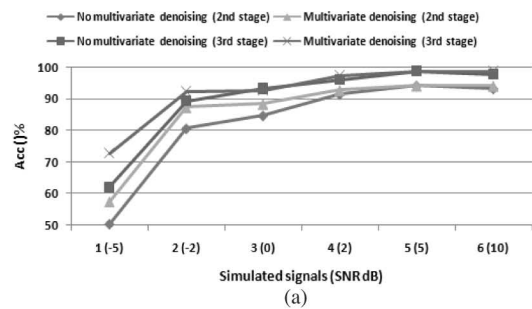
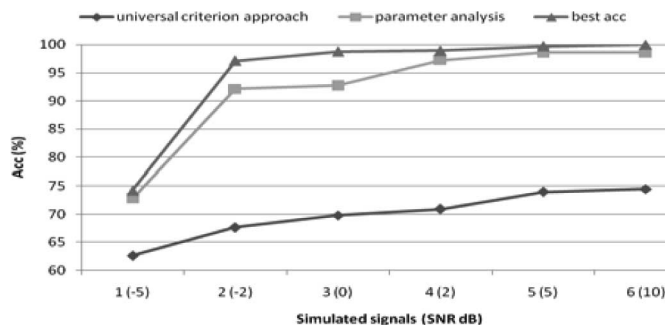


Fig. 10. Obtained Acc using the universal criterion approach, the parameter analysis, and the best Acc, for the simulated signals.

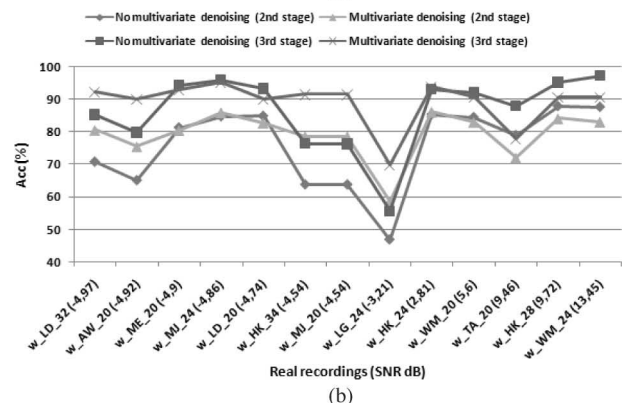
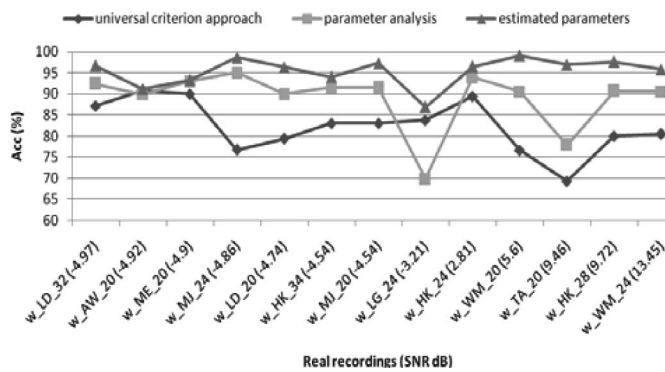


Fig. 11. Obtained Acc using the universal criterion approach, the parameter analysis, and the parameter estimation, for the real signals.

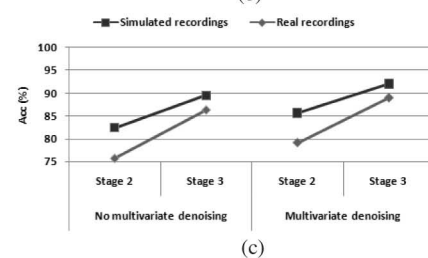


Fig. 12. Obtained Acc after multivariate denoising and the third stage of our methodology for the (a) simulated and (b) real recordings, respectively. (c) Results from the overall methodology.

R-peaks (FP) is high (227) and the corresponding classification accuracy is low (86.9%). Using the two-tailed *t*-test, the obtained *p*-value is 0.01%; thus, the difference in the classification accuracy between the universal criterion approach and the parameter estimation technique is statistically significant at a 95% confidence level.

To our knowledge, neither multivariate denoising nor 3-D phase space analysis has been previously used for fHR detection. In addition, the introduction of the a_2 , b_2 , and c_2 parameters in the 3-D phase space analysis, which is a novel feature, is a generalization of the existing technique and is motivated by the

fact that the assumption of the existing technique (i.e., the signal follows normal distribution) does not hold. Therefore, the parameters are introduced in order to optimally adjust the 3-D phase space analysis to each signal; the results indicate that the parameter introduction improves the effectiveness of the pro-

posed methodology. However, it should be mentioned that, in order to define the values of the parameters, we have to use the simulated signal's analysis. Also, the methodology is designed to integrate various denoising techniques in several of its stages; there are only few approaches presented in the literature using an embedded noise treatment strategy [1], [9], [23] while most proposed techniques do not cope with noisy recordings, and thus, cannot be used in real clinical practice. Additionally, the proposed methodology can be applied in multivariate recordings with two or more sources; the real abdECG signals used for evaluation are recorded using three leads and the simulated recordings include five, while no thoracic leads are needed. This is a major advantage of our methodology compared to BSS-based methods that require a large number of recorded leads in order to provide a reliable analysis. It should be mentioned that these methods attempt to separate fECG from mECG while our methodology extracts the fHR while, in several cases, the fHR is not extracted from the estimated fECG [3], [4], [9]–[14], [16]–[21]. The separation of mECG and fECG is a very complicated task and a more difficult procedure than extracting only mHR and fHR. However, separation is not always possible especially in signals with low SNR. The proposed methodology has no constraints related to the number of leads and its application is feasible even if only two leads are recorded. However, the recorded leads must carry sufficient fetal interference for the methodology to be applied and present sufficient accuracy.

Most of the approaches proposed in the literature, either based on BSS techniques or not, are evaluated using simulated signals [4], [8]–[10], [12], [16], [17], [19]–[22] or/and a very small dataset of real recordings [3], [4], [8]–[12], [16], [17], [19]–[21], [23], while the presented results are only qualitative [4], [8]–[11], [17]–[19], [22]; no quantitative criterion that measures the quality of the signal of interest exists. The proposed methodology has been evaluated using simulated signals with various SNR ratios and real recordings obtained from different women at various weeks of gestation. This extensive evaluation procedure is an advantage of our study, compared to several studies presented in the literature, ensuring the reliability of the obtained results that demonstrate the effectiveness and robustness of the proposed methodology. A limitation of the proposed methodology is that the short-term fHR variability is affected, since the fHR is extracted from both detected (second stage) and estimated (third stage) fetal R-peaks. However, the exact position of fetal R-peaks that overlap with maternal QRSs cannot be determined in real abdECG recordings, and thus, this limitation is present in all similar studies, either for fHR extraction or for total fECG–mECG separation.

A comparison of the results obtained by the proposed methodology and five other methods is shown in Figs. 13 and 14 for the simulated and real signals, respectively. The presented results correspond to the best channel (lead) of the analyzed signal (i.e., the lead that carries the higher fECG interference). However, it is not always possible to automatically identify the best channel; thus, a merging procedure is usually necessary. For the parabolic fitting, SNEO, template matching, and fast-ICA techniques, the identification of the best channel was made manually, while for the proposed methodology and the t-f based

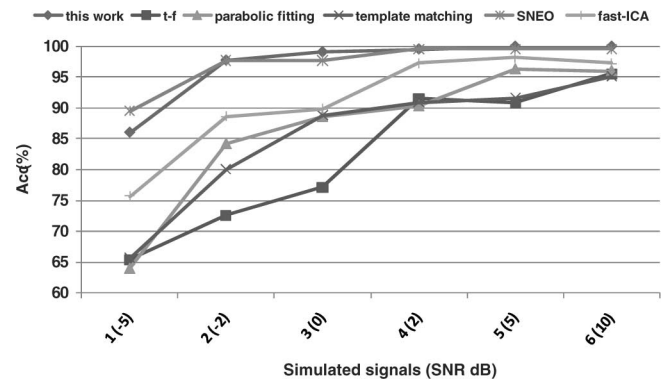


Fig. 13. Comparison of the proposed methodology (in terms of Acc) for simulated signals with five other methods.

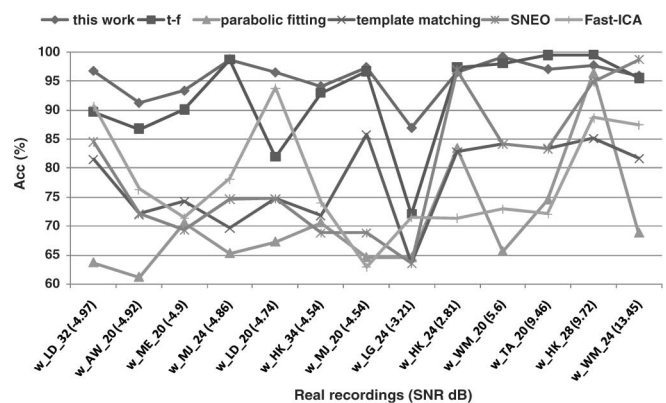


Fig. 14. Comparison of the proposed methodology (in terms of Acc) for real recordings with five other methods.

approach, a merging procedure is employed. The accuracy obtained by all techniques increases monotonically with respect to the SNR. SNEO approach performs equally well as compared to the proposed method (97.26% and 97.06%, respectively), while t-f based methodology, parabolic fitting, template matching, and fast-ICA approaches present lower results. In the case of the real recordings, the average accuracy of the proposed methodology is higher (95.45%) than the other methods. More specifically, the average obtained accuracy is 92.17%, 70.47%, 80.23%, and 78.63% for the t-f based, parabolic fitting, SNEO, and template matching methodology, respectively.

In Table VIII, several methods proposed in the literature for the extraction of the fHR are presented. Each approach is evaluated using a different dataset, since there is no benchmark database. Thus, a direct comparison between the methods is not possible. All the methods were validated using real recordings; no simulated signals were involved. In addition, all methods presented in Table VIII (including the proposed one) do not require a large number of recorded leads. The results of the proposed methodology presented in Table VIII correspond to the real recordings. In addition, the analysis in all these methods is based on abdECG recordings without including thoracic leads. Pieri *et al.* [1] use the largest dataset among all the methods presented in Table VIII (400 records of 5–10 min each), but the results

TABLE VIII
COMPARISON OF THE PROPOSED METHODOLOGY WITH OTHER WORKS USING REAL SIGNALS

Author	Description	Dataset	Accuracy (%)
Pieri <i>et al.</i> , 2001 [1]	Matched filter	400 records (3 abdominal leads) Duration: 5-10 min 8 short records (3 abdominal leads)	65
Karvounis <i>et al.</i> , 2004 [14]	Time-frequency analysis	Duration: 1 min 10 long records (3 abdominal leads)	99.19
Martens <i>et al.</i> , 2007 [15]	PCA & matched filtering	Duration: 15 min 20 long recording (13 abdominal leads)	85
Ibrahimy <i>et al.</i> , 2003 [23]	Statistical analysis	Duration: 30 min 5 records: (1 abdominal lead)	89 ¹
Azad, 2000 [24]	Fuzzy approach	Duration: 20 min 5 records: (3 abdominal leads)	89 ²
<i>Current Work</i>	<i>Phase-space</i>	13 long records (3 abdominal leads) Duration: 15 min	95.45

¹Correlation coefficient between the simultaneous fHR measured from Doppler ultrasound and the proposed methodology.

²Defined as $performance = \frac{TP - (FP + FN)}{TP} \times 100(\%)$.

are rather poor (65%). Karvounis *et al.* [14] presented high results, using a t-f based methodology, however, without any noise handling procedure; thus, the proposed methodology is a more compact approach and handles more adequately noisy and multivariate recordings. Also, the evaluation was performed using additionally simulated signals while the dataset of real recordings is larger. Martens *et al.* [15] propose a PCA-based methodology for fECG detection and the presented results are promising (85% accuracy), which, however, requires a large number of leads since they use 13 abdominal leads. The study by Ibrahimy *et al.* [23] also performs very well and is validated using five records of 20 min each, but the reported result (89%) is the correlation coefficient between the simultaneous fHR measured from Doppler ultrasound and the proposed method; no medical annotation of the fHR is included. The fuzzy-based approach by Azad [24] performs well with 89% average performance (defined as $performance = (TP - (FP + FN)/TP) \times 100(\%)$), but there is no indication on the exact number and duration of abdECG records used for the evaluation. Using the performance definition, the results of the proposed methodology are 90.1% for the simulated signals and 95.1% for the real recordings.

VII. CONCLUSION

A methodology for the automated extraction of fHR from the abdECG signal is proposed, based on multivariate denoising and 3-D phase space analysis. Six abdECG-simulated signals, being generated using different SNRs, and 13 real records, from several subjects and covering almost all of the gestation period (from the 20th to 34th week), are employed in the evaluation of the methodology and the presented results indicate high efficiency. Both multivariate analysis and 3-D phase space analysis

have not been previously employed for fHR extraction. Noise handling is also addressed, in order for the methodology to be able to cope with noisy recordings. Results of the parameter analysis indicate the dependence of the parameters used in 3-D phase space analysis on the SNR of the signal, and an approach for the estimation of these parameters is proposed. Future work will focus on the application of the methodology to other datasets and realistic conditions to fully evaluate its potential. In addition, alternative approaches related to each stage of the methodology, such as different methods for mQRS cancellation and fetal R-peak detection, will be examined. The parameter estimation approach can be further improved by using estimated values of the parameters based on a subset of real recordings instead of using simulated signals or by adaptive estimation, i.e., the values of the parameters will adapt to the short-term SNR of the abdECG signal.

ACKNOWLEDGMENT

The authors are grateful to Prof. K. K. Naka, MD, Medical School, Department of Cardiology, University of Ioannina, for her help related to the medical aspects of this research.

REFERENCES

- [1] J. F. Pieri, J. A. Crowe, B.R. Hayes-Gill, C. J. Spencer, K. Bhogal, and D. K. James, "Compact long-term recorder for the transabdominal foetal and maternal electrocardiogram," *Med. Biol. Eng. Comput.*, vol. 39, pp. 118–125, 2001.
- [2] E. M. Symond, D. Sahota, and A. Chang, *Fetal Electrocardiography*. London, U.K.: Imperial College Press, 2001.
- [3] M. Martinez, E. Soria, J. Calpe, J. F. Guerrero, and J. R. Magdalena, "Application of the adaptive impulse correlated filter for recovering fetal electrocardiogram," in *Proc. Comput. Cardiol.*, Lund, Sweden, 1997, pp. 9–12.
- [4] G. Camps-Valls, M. Martinez-Sober, E. Soria-Olivas, R. Magdalena-Benedito, J. Calpe-Maravilla, and J. Guerrero-Martinez, "Foetal ECG recovery using dynamic neural networks," *Artif. Intell. Med.*, vol. 31, pp. 197–209, 2004.
- [5] E. G. M. Golbach, J. G. Stinstra, P. Grot, and M. J. Peters, "Reference values for fetal MCG/ECG recordings in uncomplicated pregnancies," in *Proc. 12th Int. Conf. Biomagn.*, Espoo, Finland, 2000, pp. 595–598.
- [6] V. Vrins, C. Jutten, and M. Verleysen, "Sensor array and electrode selection for non-invasive fetal electrocardiogram extraction by independent component analysis," in *Proc. 5th Int. Conf., ICA 2004*, Granada, Spain, Sep. 22–24, pp. 1017–1024.
- [7] R. Sameni, G. D. Clifford, C. Jutten, and M. B. Shamsollahi, "Multichannel ECG and noise modeling: Application to maternal and fetal ECG signals," *EURASIP J. Adv. Signal Process.*, pp. 1–14, 2007, Research Article ID 43407, doi:10.1155/2007/43407.
- [8] L. D. Lathauwer, B. D. Moor, and J. Vandewalle, "Fetal electrocardiogram extraction by blind source subspace separation," *IEEE Trans. Biomed. Eng.*, vol. 47, no. 5, pp. 567–572, May 2000.
- [9] A. Al-Zaden and A. Al-Smadi, "Extraction of foetal ECG by combination of singular value decomposition and neuro-fuzzy inference system," *Phys. Med. Biol.*, vol. 51, pp. 137–143, 2006.
- [10] P. P. Kanjilal, S. Palit, and G. Saha, "Fetal ECG Extraction from single-channel maternal ECG using singular value decomposition," *IEEE Trans. Biomed. Eng.*, vol. 44, no. 1, pp. 51–59, Jan. 1997.
- [11] V. Zarzoso and A. K. Nandi, "Noninvasive fetal electrocardiogram extraction: Blind separation versus adaptive noise cancellation," *IEEE Trans. Biomed. Eng.*, vol. 48, no. 1, pp. 12–18, Jan. 2001.
- [12] M. G. Jafari and J. A. Chambers, "Fetal electrocardiogram extraction by sequential source separation in the wavelet domain," *IEEE Trans. Biomed. Eng.*, vol. 52, no. 3, pp. 390–400, Mar. 2005.
- [13] M. Sato, Y. Kimura, S. Chida, T. Ito, N. Katayama, K. Okamura, and M. Nakao, "A novel extraction method of fetal electrocardiogram from the composite abdominal signal," *IEEE Trans. Biomed. Eng.*, vol. 54, no. 1, pp. 49–58, Jan. 2007.

- [14] E. C. Karvounis, M. G. Tsipouras, D. I. Fotiadis, and K. K. Naka, "An automated methodology for fetal heart rate extraction from the abdominal electrocardiogram," *IEEE Trans. Inf. Technol. Biomed. (T-ITB)*, vol. 11, no. 6, pp. 628–638, Nov. 2007.
- [15] S. M. M. Martens, C. Rabotti, M. Mischi, and R. J. Sluijter, "A robust fetal ECG detection method for abdominal recordings," *Physiol. Meas.*, vol. 28, pp. 373–388, 2007.
- [16] A. K. Barros and A. Cichocki, "Extraction of specific signals with temporal structure," *Neural Comput.*, vol. 13, pp. 1995–2003, 2001.
- [17] Z. L. Zhang and Z. Yi, "Extraction of a source signal whose kurtosis value lies in a specific range," *Neurocomputing*, vol. 69, pp. 900–904, 2006.
- [18] M. Richter, T. Schreiber, and D. T. Kaplan, "Fetal ECG extraction with nonlinear state space projections," *IEEE Trans. Biomed. Eng.*, vol. 45, no. 1, pp. 133–137, Jan. 1998.
- [19] K. Assaleh and H. Al-Nashash, "A novel technique for the extraction of fetal ECG using polynomial networks," *IEEE Trans. Biomed. Eng.*, vol. 52, no. 6, pp. 1148–1152, Jun. 2005.
- [20] K. Assaleh, "Extraction of fetal electrocardiogram using adaptive neuro-fuzzy inference systems," *IEEE Trans. Biomed. Eng.*, vol. 54, no. 1, pp. 59–68, Jan. 2007.
- [21] A. Khamene and S. Negahdaripour, "A new method for the extraction of fetal ECG from the composite abdominal signal," *IEEE Trans. Biomed. Eng.*, vol. 47, no. 4, pp. 507–516, Apr. 2000.
- [22] A. K. Barros, "Extracting the fetal heart rate variability using a frequency tracking algorithm," *Neurocomputing*, vol. 49, pp. 279–288, 2002.
- [23] M. I. Ibrahimy, F. Ahmed, M. A. M. Ali, and E. Zahedi, "Real-time signal processing for fetal heart rate monitoring," *IEEE Trans. Biomed. Eng.*, vol. 50, no. 2, pp. 258–262, Feb. 2003.
- [24] K. A. K. Azad, "Fetal QRS complex detection from abdominal ECG: A fuzzy approach," in *Proc. IEEE Nordic Signal Process. Symp.*, Kolmarden, Sweden, 2000, pp. 275–278.
- [25] Q. Zhang, "MATLAB package for robust and efficient location of T-wave ends in ECG and its evaluation with physionet data," 2005. [Online]. Available: <http://www.irisa.fr/sosso/zhang/biomedical/>
- [26] D. G. Goring and V. I. Nikora, "Despiking acoustic Doppler velocimeter data," *J. Hydr. Eng.*, vol. 128, pp. 117–126, 2002.
- [27] T. L. Wahl, "Discussion of 'despiking acoustic doppler velocimeter data' by Derek G. Goring and Vladimir I. Nikora," *J. Hydr. Eng.*, vol. 129, pp. 487–488, 2003.
- [28] N. Mori, T. Suzuki, and S. Kakuno, "Noise of acoustic Doppler velocimeter data in bubbly flow," *J. Eng. Mech.*, vol. 133, pp. 122–125, 2007.
- [29] B. R. Bakshi, "Multiscale PCA with application to multivariate statistical process monitoring," *AIChE J.*, vol. 44, pp. 1596–1610, 1998.
- [30] D. Wang and J. Romagnoli, "Robust multi-scale principal components analysis with applications to process monitoring," *J. Process Control*, vol. 15, pp. 869–882, 2005.
- [31] M. Aminghafari, N. Cheze, and J. M. Poggi, "Multivariate de-noising using wavelets and principal component analysis," *Comput. Stat. Data Anal.*, vol. 50, pp. 2381–2398, 2006.
- [32] R. Sameni, "Open Source ECG toolbox—Multi-channel Synthetic ECG Generator, version 1.0," Nov. 2006 [Online]. Available: <http://ecg.sharif.edu/SyntheticECGTools.htm>
- [33] S. Abboud and D. Sadeh, "Spectral analysis of the fetal electrocardiogram," *Comput. Biol. Med.*, vol. 19, pp. 409–415, 1989.
- [34] F. L. Foresta Azzerboni, N. Mammoni, and F. C. Morabito, "A new approach based on wavelet-ICA Algorithms for fetal electrocardiogram extraction," in *Proc. 13th Eur. Symp. Artif. Neural Netw.*, Bruges, Belgium, 2005, pp. 27–29.
- [35] N. M. Gibson, M. S. Woolfson, and J. A. Crowe, "Detection of fetal electrocardiogram signals using matched filters with adaptive normalization," *Med. Biol. Eng. Comput.*, vol. 35, pp. 216–222, 1997.
- [36] J. F. Guerrero-Martínez, M. Martínez-Sober, M. Bataller-Mompean, and J. R. Magdalena-Benedito, "New algorithm for fetal QRS detection in surface abdominal records," in *Proc. Comput. Cardiol.*, Valencia, Spain: IEEE Comput. Soc. Press, 2006, pp. 441–444.
- [37] A. Hyvarinen, "Fast and robust fixed point algorithm for independent component analysis," *IEEE Trans. Neural Netw.*, vol. 10, no. 3, pp. 626–634, May 1999.



Evaggelos C. Karvounis (M'07) was born in Ioannina, Greece, in 1978. He received the Diploma degree in computer science from the University of Thessaloniki, Thessaloniki, Greece, in 2002. He is currently working toward the Ph.D. degree in the Department of Materials Science and Engineering, University of Ioannina, Ioannina.

His current research interests include biomedical engineering, decision support systems in healthcare, and biomedical applications.



Markos G. Tsipouras (M'07) was born in Athens, Greece, in 1977. He received the Diploma degree and the M.Sc. degree in computer science from the University of Ioannina, Ioannina, Greece, in 1999 and 2002, respectively. He is currently working toward the Ph.D. degree in the Department of Computer Science, University of Ioannina.

His current research interests include biomedical engineering, decision support and medical expert systems, and biomedical applications.



Dimitrios I. Fotiadis (M'01–SM'07) was born in Ioannina, Greece, in 1961. He received the Diploma degree in chemical engineering from the National Technical University of Athens, Athens, Greece, in 1985, and the Ph.D. degree in chemical engineering from the University of Minnesota, Minneapolis, in 1990.

From 1995 to early 2008, he was with the Department of Computer Science, University of Ioannina, where he is currently a Professor in the Department of Materials Science and Technology. He is the Director of the Unit of Medical Technology and Intelligent Information Systems and President of the Science and Technology Park of Epirus, Greece. His current research interests include biomedical technology, biomechanics, scientific computing, and intelligent information systems.